Thermoelectricity in Molecular Junctions

Pramod Reddy, *et al.*

Science **315**, 1568 (2007);
DOI: 10.1126/science.1137149

22. H. O. Finklea, D. D. Hanshew, *J. Am. Chem. Soc.* **114**, 3173 (1992).
23. J. P. Collman, N. K. Devaraj, T. P. A. Eberspacher, C. E. D. Chidsey, *Langmuir* **22**, 2457 (2006).
24. J. P. Collman, N. K. Devaraj, C. E. D. Chidsey, *Langmuir* **20**, 1051 (2004).
25. J. K. Lee, Y. S. Chi, I. S. Choi, *Langmuir* **20**, 3844 (2004).
26. V. V. Rostovtsev, L. G. Green, V. V. Fokin, K. B. Sharpless, *Angew. Chem. Int. Ed.* **41**, 2596 (2002).
27. C. W. Tornoe, C. Christensen, M. Meldal, *J. Org. Chem.* **67**, 3057 (2002).
28. N. K. Devaraj, R. A. Decreau, W. Ebina, J. P. Collman, C. E. D. Chidsey, *J. Phys. Chem. B* **110**, 15955 (2006).
29. Materials and methods are available as supporting material on *Science* Online.
30. R. Boulatov, J. P. Collman, I. M. Shiryaeva, C. J. Sunderland, *J. Am. Chem. Soc.* **124**, 11923 (2002).
31. A. S. Haas *et al.*, *J. Phys. Chem. B* **105**, 11351 (2001).
32. S. K. Cha, *Bull. Korean Chem. Soc.* **25**, 786 (2004).
33. T. H. Degefa, P. Schon, D. Bongard, L. Walder, *J. Electroanal. Chem.* **574**, 49 (2004).
34. E. Katz, H. L. Schmidt, *J. Electroanal. Chem.* **368**, 87 (1994).
35. J. A. Sigman, B. C. Kwok, Y. Lu, *J. Am. Chem. Soc.* **122**, 8192 (2000).
36. G. T. Babcock, M. Wikstrom, *Nature* **356**, 301 (1992).
37. J. P. Collman, R. Boulatov, *Angew. Chem. Int. Ed.* **41**, 3487 (2002).
38. The peroxide detected at the ring electrode could arise either from direct release of peroxide during the catalytic cycle or from release and rapid disproportionation of superoxide (*42*). The hydrolytic autoxidation of heme oxygen complexes in aqueous solution is a well-documented phenomenon (*39*, *43*). This process is known to be catalyzed by protons, and preliminary results indicate that the selectivity of all of our catalysts can be markedly improved by raising the pH (to the range of 8 to 12). Furthermore, our prior work with CcO models on edge-plane graphite provided evidence that superoxide is a substantial source of PROS (*30*).
39. K. Shikama, *Chem. Rev.* **98**, 1357 (1998).
40. S. E. Creager, G. K. Rowe, *Langmuir* **9**, 2330 (1993).
41. G. B. Sigal, M. Mrksich, G. M. Whitesides, *Langmuir* **13**, 2749 (1997).
42. D. T. Sawyer, J. S. Valentine, *Acc. Chem. Res.* **14**, 393 (1981).
43. J. P. Collman, Y. L. Yan, T. Eberspacher, X. J. Xie, E. I. Solomon, *Inorg. Chem.* **44**, 9628 (2005).
44. We dedicate this scientific contribution to the memory of the late H. Taube. We thank J. I. Brauman, T. D. P. Stack, C. C. Cummins, R. Boulatov, and P. H. Dinolfo for helpful discussions. N.K.D., R.A.D., and W.E. acknowledge a Stanford graduate fellowship, a Lavoisier fellowship, and a Dreyfus undergraduate fellowship, respectively. This material has its basis in work supported by the NIH under grant GM-17880-35.

Supporting Online Material

www.sciencemag.org/cgi/content/full/315/5818/1565/DC1
Materials and Methods
Figs. S1 to S4
References

3 October 2006; accepted 23 January 2007
10.1126/science.1135844

Thermoelectricity in Molecular Junctions

Pramod Reddy,[1]* Sung-Yeon Jang,[2,3]*† Rachel A. Segalman,[1,2,3]‡ Arun Majumdar[1,3,4]‡

By trapping molecules between two gold electrodes with a temperature difference across them, the junction Seebeck coefficients of 1,4-benzenedithiol (BDT), 4,4′-dibenzenedithiol, and 4,4″-tribenzenedithiol in contact with gold were measured at room temperature to be +8.7 ± 2.1 microvolts per kelvin (μV/K), +12.9 ± 2.2 μV/K, and +14.2 ± 3.2 μV/K, respectively (where the error is the full width half maximum of the statistical distributions). The positive sign unambiguously indicates p-type (hole) conduction in these heterojunctions, whereas the Au Fermi level position for Au-BDT-Au junctions was identified to be 1.2 eV above the highest occupied molecular orbital level of BDT. The ability to study thermoelectricity in molecular junctions provides the opportunity to address these fundamental unanswered questions about their electronic structure and to begin exploring molecular thermoelectric energy conversion.

Study of charge transport in molecules is of fundamental interest, with potential applications in molecular electronics (*1*) and energy-conversion devices (*2*, *3*). Current-voltage (I-V) characteristics of single molecules have been extensively investigated by trapping a single molecule in break junctions formed by mechanical strain (*4*), electromigration (*5*), and scanning tunneling microscopes (*6*). Although such measurements have provided substantial insight into charge transport through molecular junctions, critical aspects about the electronic structure cannot be uniquely obtained by I-V characteristics alone. For example, whether molecular junctions are p-type or n-type—i.e., whether the position of the Fermi level, E_F, of the metal contacts is closer to the highest occupied molecular orbital (HOMO) or to the lowest unoccupied molecular orbital (LUMO)—generally remains unknown because of uncertainties in the microscopic details of the contacts (*7*–*10*). A specific example of this is benzenedithiol (BDT); in this case, although the electrical conductance has been studied extensively both experimentally (*4*, *11*) and theoretically (*7*, *12*–*15*), some groups suggest that the E_F of the electrodes lies close to the HOMO level (*7*, *13*, *15*) and other groups contend that E_F lies near the LUMO level (*12*, *14*). Although sweeping the gate bias in single-molecule transistors could potentially yield this information, Coulombic interactions caused by charge accumulation on the molecule could perturb the electronic structure (*16*, *17*).

It has been suggested that the sign of the Seebeck coefficient, *S*, of molecular junctions can indicate the sign of the charge carrier and the relative position of E_F with respect to the HOMO or LUMO levels (*8*). Indeed, thermopower measurements that use a scanning probe microscope have yielded nanoscale spatial distributions of electron and hole concentrations in inorganic semiconductors (*18*) and have led to chemical potential microscopy at the atomic scale (*19*, *20*). Here, we report an alternative approach: We measured *S* for molecular junctions formed by trapping molecules between gold electrodes, and then we measured the voltage generated across them when a temperature bias was imposed across the junction.

In general, *S* is associated with bulk materials and is obtained by measuring the voltage difference created across a material in response to an applied temperature differential. In such bulk materials, charge transport is diffusive in nature. The concept of an effective *S* is also valid for junctions where the transport may be ballistic. For such junctions, however, a more general form of the Seebeck coefficient is needed and is given as

$$S = \frac{1}{eT}\frac{\int_0^\infty \sigma(E)(E - E_F)dE}{\int_0^\infty \sigma(E)dE} \quad (1)$$

where $\sigma(E)$ is the energy-dependent differential electrical conductivity, E_F is the Fermi level (or more accurately, the chemical potential), e is the charge of an electron, and T is the absolute temperature; the denominator in Eq. 1 is the electrical conductivity, σ. As Eq. 1 suggests, *S* reflects the asymmetry in $\sigma(E)$ with respect to E_F. In bulk materials, this asymmetry results from energy-dependent carrier scattering or the asymmetry in the density of states. For ballistic transport, the asymmetry can be created by a potential barrier at a junction, such as that created between E_F of a metal and the HOMO or LUMO level of a molecule. Here, *S* is not an intrinsic property of a material, but that of the heterojunction. Hence, we call it a junction Seebeck coefficient, $S_{junction}$. Because $S_{junction}$

[1]Applied Science and Technology Program, University of California, Berkeley, CA 94720, USA. [2]Department of Chemical Engineering, University of California, Berkeley, CA 94720, USA. [3]Materials Science Division, Lawrence Berkeley Laboratory, Berkeley, CA 94720, USA. [4]Departments of Mechanical Engineering and Materials Science and Engineering, University of California, Berkeley, CA 94720, USA.

*These authors contributed equally to this paper.
†Present address: Optoelectronic Materials Research Center, Korea Institute of Science and Technology, Seoul 136-791, Korea.
‡To whom correspondence should be addressed. E-mail: majumdar@me.berkeley.edu (A.M.); segalman@berkeley.edu (R.A.S.)

measures the size of an energy barrier, it is not expected to depend on the number of molecules trapped between the electrodes and is, therefore, an intrinsic property of the junction. This is in contrast to the junction's electrical conductance, which depends on the number of molecules.

A modified scanning tunneling microscope (STM) setup is shown schematically in Fig. 1A: A customized control circuit drives a Au STM tip at a constant speed toward a Au substrate in air under ambient conditions. The Au tip is kept in contact with a large thermal reservoir at room temperature, which maintains the tip temperature very close to ambient (*21*–*23*). The Au substrate can be heated with an electric heater to a desired temperature above ambient to create a tip-substrate temperature difference, ΔT. When the Au STM tip approaches the hot substrate, a tip-substrate voltage bias is applied and the current is continuously monitored. When the conductance reaches a sufficiently high threshold of $0.1G_o$, where $G_o = 2e^2/h$ is the quantum of charge conductance [see (*23*) for a discussion on the choice of $0.1G_o$], our previous experiments on electrical conductance have shown that the tip-substrate distance is sufficient to trap molecules between the electrodes (*24*). Once this threshold is reached, the voltage bias and the current amplifier are disconnected, and the voltage amplifier is connected instead (Fig. 1A) to measure the tip-substrate thermoelectric voltage induced by ΔT. The tip is then slowly withdrawn to a sufficiently large distance (~15 nm) and the output voltage ΔV is continuously monitored with the tip grounded.

When the Au substrate is covered by thiol-terminated molecules, we have shown that molecular bridges are formed between the Au tip and the substrate, and the electrical conductance of single molecules can be monitored in air (*24*). In our experiment, we covered the Au substrate with BDT, dibezenedithiol (DBDT), or tribenzenedithiol (TBDT) (*25*) molecules. If molecules of BDT, DBDT, or TBDT are trapped between the tip and substrate with a superimposed ΔT, we should expect to see a thermoelectric voltage generated between the electrodes (*8*), which should last as long as one or more molecules are trapped and vanish once all of the molecules break away.

A typical thermoelectric voltage curve obtained in the experiment that was performed with a ΔT of 20 K and with the substrate covered with BDT molecules is shown in Fig. 1B. We observed a constant thermoelectric voltage of about $\Delta V = -200$ μV (Fig. 1B, blue curve), which lasted until all of the molecules trapped in the junction broke away. Notably, the distance the tip travels (~ 1 to 2 nm) before all of the molecules break away is much longer than the molecular length. Because the thiol group on the molecule binds sufficiently strongly to Au, and because Au atoms are sufficiently mobile at room temperature, it has been proposed that Au chains are formed both on the tip and the substrate when the STM tip is pulled away (*6*). In contrast to electrical conductance measurements (*24*), which decrease in steps as molecules break away one at a time, no steps were observed in the ΔV, suggesting that $S_{junction}$ is independent of the number of molecules. As the ΔT increases from 0 to 30 K, the thermoelectric voltage signal increases (Fig. 1C). Control experiments performed on clean gold surfaces without any molecules (red, Fig. 1B) demonstrate that no measurable ΔV is generated in the absence of molecules.

To obtain a statistically significant value of ΔV of a Au-BDT-Au junction, we performed roughly 1000 consecutive experiments at each value of ΔT. These data were used to construct histograms for each temperature differential without any data preselection. The histograms thus obtained (Fig. 2, A to C) were used to estimate the average and the variation in $S_{junction}$. The relation between $S_{junction}$ of the Au-molecule-Au junction and the measured voltage is (*23*)

$$S_{junction} = S_{Au} - \frac{\Delta V}{\Delta T} \qquad (2)$$

where S_{Au} is the Seebeck coefficient of bulk Au, which is ~1.94 μV/K at 300 K (*26*). In Fig. 2D, ΔV_{peak} is plotted as a function of ΔT, where ΔV_{peak} corresponds to the ΔV at the peak of the distribution. The error bars in Fig. 2D correspond to the full-width half-maximum (FWHM) of the distributions. From the slope $\Delta V_{peak}/\Delta T$ and Eq. 2, one obtains $S_{Au\text{-}BDT\text{-}Au} = +8.7 \pm 2.1$ μV/K, where the error is FWHM. Similar experiments were also performed with DBDT and TBDT, and statistical analysis revealed that $S_{Au\text{-}DBDT\text{-}Au} = +12.9 \pm 2.2$ μV/K and $S_{Au\text{-}TBDT\text{-}Au} = +14.2 \pm 3.2$ μV/K (*23*) (Fig. 2E). There seems to be a linear dependence of thermopower with molecular length, which is in contrast to the exponential dependence of electrical resistance that is generally attributed to tunneling across the molecule. The histograms of ΔV for Au-TBDT-Au junctions at 20 and 30 K (fig. S4, A to C) exhibit deviations from a Gaussian curve. Furthermore, the FWHMs for the histograms at 20 and 30 K increased considerably compared with those of Au-BDT-Au junctions, which may arise from the effect of the conformational changes in the molecules trapped in the junctions. The plot of the peak values of the histograms versus the temperature differential for DBDT and TBDT (figs. S3D and S4D) show deviations from linearity. This deviation may arise because the applied temperature differentials of 20 and 30 K across molecules are so high that linear transport theory may not adequately describe the temperature dependence of the thermoelectric voltage.

The relative position of the HOMO and LUMO levels with respect to the E_F of the metal

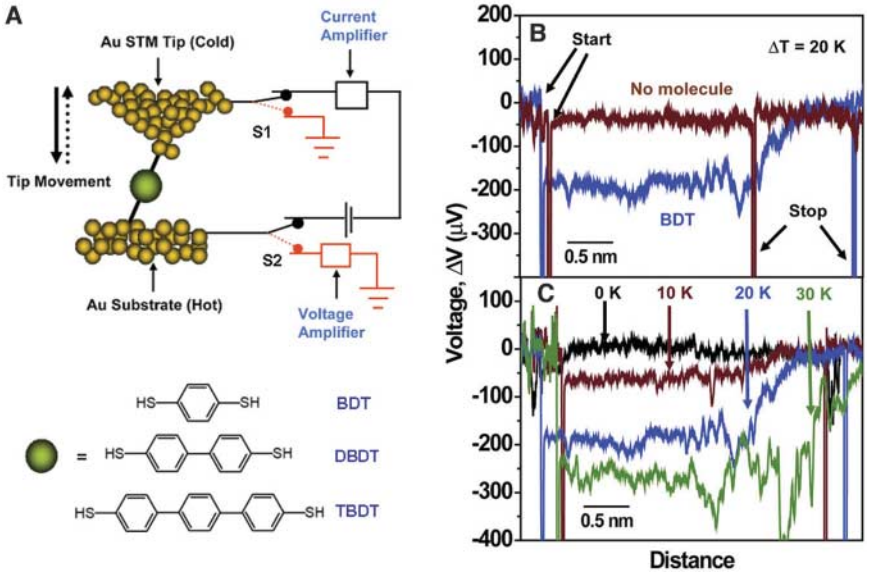

Fig. 1. Experimental setup and measurements. (**A**) Schematic description of the experimental set up based on an STM break junction. Molecules of BDT, DBDT, or TBDT are trapped between the Au STM tip kept at ambient temperature and a heated Au substrate kept at temperature ΔT above the ambient. When the tip approaches the substrate, a voltage bias is applied and the current is monitored to estimate the conductance. When the conductance reaches a threshold of $0.1G_o$, the voltage bias and the current amplifier are disconnected. A voltage amplifier is then used to measure the induced thermoelectric voltage, ΔV, and the tip is gradually pulled away from the substrate. (**B**) A plot of the thermoelectric voltage measured as a function of the tip-sample distance when a temperature differential $\Delta T = 20$ K is applied (Au tip at ambient and substrate at ambient + 20 K). The blue curve is obtained when a Au-BDT-Au junction is broken. The red curve shows a control experiment performed on a clean gold substrate. (**C**) Typical thermoelectric voltage traces for tip-substrate temperature differentials of 0, 10, 20, and 30 K for Au-BDT-Au junctions.

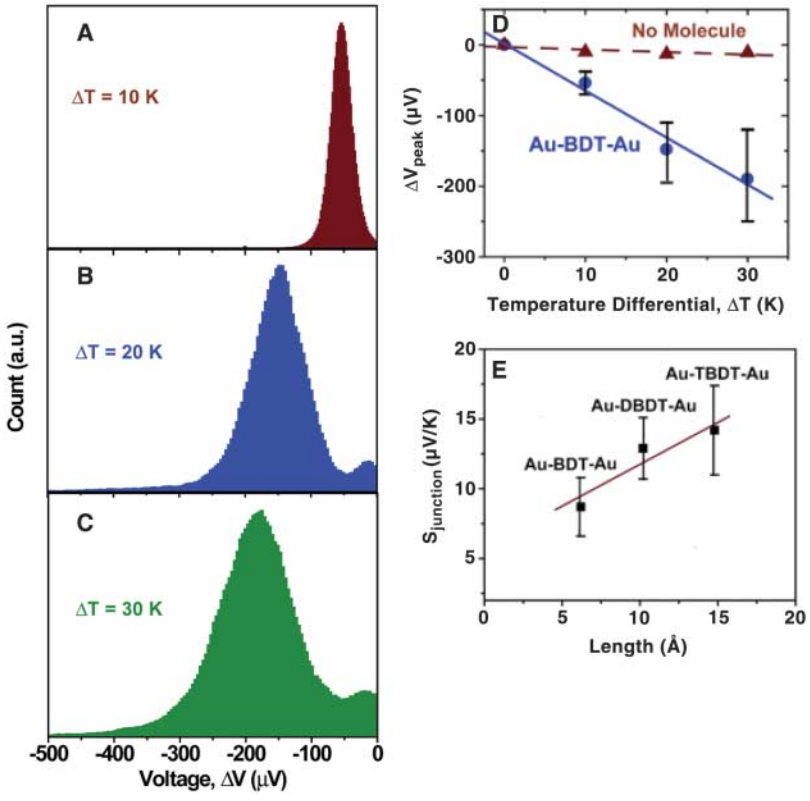

Fig. 2. Histograms obtained by analyzing approximately 1000 consecutive thermoelectric voltage curves obtained in measurements of Au-BDT-Au junctions with tip-substrate temperature differential (**A**) ΔT = 10 K, (**B**) ΔT = 20 K, and (**C**) ΔT = 30 K. a.u., arbitrary units. (**D**) Plot of the peak values of the thermoelectric voltage in histograms as a function of the temperature differential. The error bars represent FWHM of the corresponding histograms. It can be seen that the measured voltage varies linearly with the temperature differential, as expected. (**E**) Plot of measured junction Seebeck coefficient as a function of molecular length for BDT, DBDT, and TBDT.

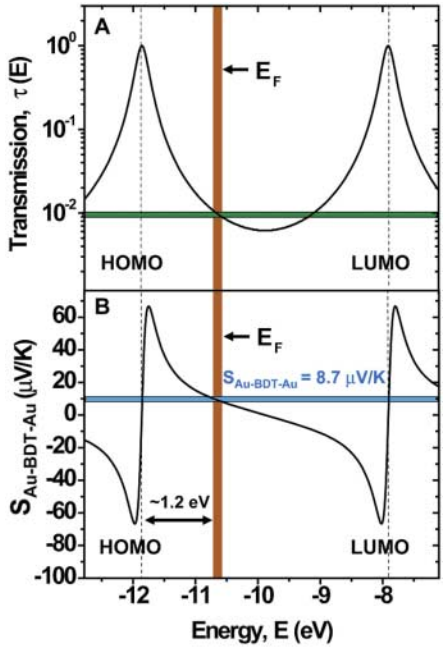

Fig. 3. Relating the measured Seebeck coefficient of Au-BDT-Au junction to the position of Fermi level. (**A**) Theoretical prediction (*8*) of the transmission function of a Au-BDT-Au junction plotted as a function of the relative position of the Fermi level of the Au electrodes with respect to the HOMO and LUMO levels. (**B**) The predicted (*8*) Seebeck coefficient of a Au-BDT-Au junction as a function of the relative position of the Fermi level with respect to the HOMO and LUMO levels. When the measured value of $S_{\text{Au-BDT-Au}}$ = +8.7 ± 2.1 μV/K (blue band) is shown, it is clear that the Fermi level is ~1.2 eV above the HOMO level. At this energy level, the transmission function is $\tau(E) \sim 0.01$.

electrodes can be related to the measured value of S_{junction} (*8*). The Landauer formula (*27*) is used to relate S_{junction} to the transmission function, $\tau(E)$. It is shown that S_{junction} can be obtained as

$$S_{\text{junction}} = -\frac{\pi^2 k_B^2 T}{3e}\frac{\partial \ln(\tau(E))}{\partial E}\bigg|_{E=E_F} \quad (3)$$

where k_B is the Boltzmann constant.

The transmission function for the case of Au-BDT-Au junction, which was derived with the use of the nonequilibrium Green's function formalism in conjunction with extended Huckel theory (*8*), is shown in Fig. 3A. It is clear that $\tau(E) \sim 1$ when the E_F aligns with either the HOMO or the LUMO levels and decreases rapidly to below 0.01 in between. Using this transmission function in Eq. 3, we calculated $S_{\text{Au-BDT-Au}}$ (Fig. 3B) and found that $S_{\text{Au-BDT-Au}}$ is positive (p-type) if E_F is closer to the HOMO level and negative (n-type) if it is closer to the LUMO level. Using the measured value of $S_{\text{Au-BDT-Au}}$ = +8.7 ± 2.1 μV/K, we see from Fig. 3B that E_F is ~1.2 eV from the HOMO level. The value of the transmission function at this relative position of the Fermi level was $\tau(E) \sim 0.01$ (Fig. 3A). In the Landauer formalism, we know that the conductance G_{molecule} can be related to the transmission function at E_F as

$$G_{\text{molecule}} \approx \frac{2e^2}{h}\tau(E)|_{E=E_F} = \tau(E)|_{E=E_F} G_o \quad (4)$$

Equation 4 implies that the conductance of BDT should be $\sim 0.01 G_o$. This estimated value of the electrical conductance is in excellent agreement with the measured electrical conductance of Au-BDT-Au junction (*11*, *28*).

Junction Seebeck coefficient measurements can provide insight into the electronic structure of the heterojunction, but the results also bear on an as-yet unexplored field of thermoelectric energy conversion based on molecules. The best efficiency in thermoelectric energy conversion can be achieved if charge transport occurs through a single energy level (*29*, *30*). Single-level transport is, however, difficult to realize in inorganic materials. Metal-molecule-metal heterojunctions are ideal in this regard because they (i) provide transport either through the HOMO or LUMO levels and (ii) have very low vibrational heat conductance because of large mismatch of vibrational spectra between the bulk metal and discrete molecules (*31*). Hence, such a hybrid material offers the promise of efficient thermoelectric energy conversion. We show for the first time values for molecular junction Seebeck coefficients, but the tunability of this effect and electrical conductance remains unknown. The length dependence of molecular junction Seebeck coefficients is shown in Fig. 2E for the molecules we studied, but there may be other ways of tuning thermopower, such as by introducing various chemical moieties in the molecule or by controlling the metal-molecule chemical bond.

References and Notes

1. A. Aviram, M. A. Ratner, *Chem. Phys. Lett.* **29**, 277 (1974).
2. W. U. Huynh, J. J. Dittmer, A. P. Alivisatos, *Science* **295**, 2425 (2002).
3. G. Yu, J. Gao, J. C. Hummlen, F. Wudl, A. J. Heeger, *Science* **270**, 1789 (1995).
4. M. A. Reed, C. Zhou, C. J. Muller, T. P. Burgin, J. M. Tour, *Science* **278**, 252 (1997).
5. H. Park *et al.*, *Nature* **407**, 57 (2000).
6. B. Xu, N. J. J. Tao, *Science* **301**, 1221 (2003).
7. P. Damle, A. W. Ghosh, S. Datta, *Chem. Phys.* **281**, 171 (2002).
8. M. Paulsson, S. Datta, *Phys. Rev. B* **67**, 241403 (2003).

9. F. Zahid, A. W. Ghosh, M. Paulsson, E. Polizzi, S. Datta, *Phys. Rev. B* **70**, 245317 (2004).
10. Consider a molecule strongly bound to one electrode and very weakly bound to the other. An example of this is scanning tunneling spectroscopy; the tip is weakly interacting with the molecule, which is strongly bound to a substrate. Under bias, such a configuration produces asymmetric I-V curves because the chemical potential of the tip crosses the HOMO and LUMO levels of the molecule, whereas that of the substrate is pinned to the molecular levels. Hence, by applying a tip bias, one can determine the chemical potential position with respect to the HOMO and LUMO levels. However, to make realistic molecular devices, the molecule cannot be weakly bound to one electrode, given that otherwise the device would be mechanically unstable and electrically irreproducible because of uncertainties of the contact. But in the case of a molecule strongly bound to both the electrodes, the chemical potential of both of electrodes is pinned and hence, symmetric I-V curves are produced under bias (*9*). This symmetry in the I-V characteristics makes it impossible to determine whether transport is through HOMO or LUMO levels (*9*).
11. X. Y. Xiao, B. Q. Xu, N. J. Tao, *Nano Lett.* **4**, 267 (2004).
12. M. Di Ventra, S. T. Pantelides, N. D. Lang, *Phys. Rev. Lett.* **84**, 979 (2000).
13. E. G. Emberly, G. Kirczenow, *Phys. Rev. B* **58**, 10911 (1998).
14. J. G. Kushmerick *et al.*, *Phys. Rev. Lett.* **89**, 086802 (2002).
15. J. Taylor, M. Brandbyge, K. Stokbro, *Phys. Rev. Lett.* **89**, 138301 (2002).
16. W. Liang, M. P. Shores, M. Bockrath, J. R. Long, H. Park, *Nature* **417**, 725 (2002).
17. J. Park *et al.*, *Nature* **417**, 722 (2002).
18. H. K. Lyeo *et al.*, *Science* **303**, 816 (2004).
19. C. C. Williams, H. K. Wickramasinghe, *Nature* **344**, 317 (1990).
20. J. C. Poler, R. M. Zimmerman, E. C. Cox, *Langmuir* **11**, 2689 (1995).
21. One might suspect that the heat flow from the substrate to the tip would cause the tip temperature to increase. However, tip-substrate heat transport is mostly due to conduction through air (thermal conductance through the molecules trapped in between the tip and the substrate or through a liquid meniscus, if present, is very small in comparison) (*22*). Because the tip-sample thermal resistance is sufficiently larger than that between the Au tip and the thermal reservoir, the Au tip will be at the reservoir temperature. Our group has previously shown this to be true (*22*). Further analysis that supports the idea that the tip is at ambient temperature is provided in (*23*). Hence, the temperature difference applied across the substrate and the reservoir is the same as that across the tip-substrate junction.
22. L. Shi, A. Majumdar, *J. Heat. Trans.* **124**, 329 (2002).
23. Materials and methods are available as supporting material on *Science* Online.
24. S. Y. Jang, P. Reddy, A. Majumdar, R. A. Segalman, *Nano Lett.* **6**, 2362 (2006).
25. B. de Boer *et al.*, *Langmuir* **19**, 4272 (2003).
26. F. J. Blatt, *Thermoelectric Power of Metals* (Plenum Press, New York, 1976), pp. xv, 264.
27. M. Buttiker, Y. Imry, R. Landauer, S. Pinhas, *Phys. Rev. B* **31**, 6207 (1985).
28. Paulsson and Datta (*8*) used the measurements of Poler *et al*. (*20*) for an asymmetric junction to predict the position of E_F with respect to HOMO and LUMO levels of a monolayer.
29. G. D. Mahan, J. O. Sofo, *Proc. Natl. Acad. Sci. U.S.A.* **93**, 7436 (1996).
30. T. E. Humphrey, H. Linke, *Phys. Rev. Lett.* **94**, 096601 (2005).
31. R. Y. Wang, R. A. Segalman, A. Majumdar, *Appl. Phys. Lett.* **89**, 173113 (2006).

32. We acknowledge support from NSF under grant no. EEC-0425914, the NSF–Nanoscale Science and Engineering Center (NSEC) Center of Integrated Nanomechanical Systems, the Berkeley–Industrial Technology Research Institute (ITRI, Taiwan) Research Center, and the Department of Energy Basic Energy Sciences (DOE-BES) Thermoelectrics Program and DOE-BES Plastic Electronics Program at the Lawrence Berkeley National Laboratory.

Supporting Online Material

www.sciencemag.org/cgi/content/full/1137149/DC1
Materials and Methods
Figs. S1 to S6
References

3 November 2006; accepted 29 January 2007
Published online 15 February 2007;
10.1126/science.1137149
Include this information when citing this paper.

The Evolutionary Demography of Ecological Change: Linking Trait Variation and Population Growth

Fanie Pelletier,[1] Tim Clutton-Brock,[2] Josephine Pemberton,[3] Shripad Tuljapurkar,[4] Tim Coulson[1]*

Population dynamics and evolutionary change are linked by the fundamental biological processes of birth and death. This means that population growth may correlate with the strength of selection, whereas evolutionary change can leave an ecological signature. We decompose population growth in an age-structured population into contributions from variation in a quantitative trait. We report that the distribution of body sizes within a population of Soay sheep can markedly influence population dynamics, accounting for up to one-fifth of observed population growth. Our results suggest that there is substantial opportunity for evolutionary dynamics to leave an ecological signature and visa versa.

Ecological and evolutionary processes have traditionally been considered to operate at such different time scales that ecologists could ignore evolutionary dynamics, while evolutionary biologists could overlook ecological processes (*1*). Recently, however, there has been growing interest in the effects that ecological and evolutionary processes have on each other (*2*–*4*). For example, genetic variation at one allozyme locus influences population dynamics in a butterfly metapopulation (*5*), and evolutionary change in body and beak size has contributed more than ecological processes to population growth in a Darwin's finch (*4*). In parallel, evolutionary biologists have shown that selection can fluctuate with ecological processes and that this can generate evolutionary change. In the same population of Darwin's finch that was the focus of (*4*), varying ecological conditions in different decades impacted on the strength, direction, and outcome of selection (*6*). Given that ecological and evolutionary processes are intertwined, it is necessary to develop methods to capture their relation. A first step in doing this is to characterize the association between the phenotypic variation on which selection operates and population growth (*7*). Here we ask how quantitative trait variation impacts population growth in a population of Soay sheep (*8*) and how selection varies with population growth.

The population of Soay sheep on Hirta, St. Kilda, has been studied in detail since 1985 (*8*). The structure and size of the population is known for each year (fig. S1). Birth weight (kg) is collected each spring, and adult body weight (kg) and hind leg length (mm)—a measure of skeletal size—are collected annually from individuals caught in the summer catch (on average ~50% of the population) (*9*). The sheep year runs from 1 August to 31 July, and recruitment is calculated as the number of lambs an individual produced in April that are still alive in August. Paternity is assigned using genetic markers to ~60% of lambs with >80% confidence (*10*). Significant age- or environment-specific additive genetic variance exists for birth weight, August body weight, and hind leg length (*8*, *11*, *12*). We estimate heritabilities, h^2 (*13*), using these values and the phenotypic variance estimated from our data set [supporting online material (SOM)].

To link variation in a quantitative trait to population growth requires an understanding of how variation in the trait influences survival and recruitment and how survival and recruitment influence population growth (*14*). One way of doing this is to calculate the proportion of variation in individual contributions to population growth, $p_{t(i)}$, accounted for by a quantitative trait. $p_{t(i)}$ is calculated as the difference between observed population growth and population growth calculated with the contribution of a focal individual removed (*15*). This quantity describes

[1]Division of Biology and the Natural Environment Research Council (NERC) Centre for Population Biology, Imperial College London, Silwood Park, Ascot, Berkshire, SL5 7PY, UK. [2]Department of Zoology, University of Cambridge, Downing Street, Cambridge, CB2 3E], UK. [3]Institute of Evolutionary Biology, University of Edinburgh, West Mains Road, Edinburgh, EH9 3JT, UK. [4]Department of Biological Sciences, Stanford University, Stanford, CA 94305–5020, USA.

*To whom correspondence should be addressed. E-mail: t.coulson@imperial.ac.uk